

Synthesis, Spectral Studies and Quantum-Chemical Investigations on the Powerful Fluorophores: Imidazo[4,5-*a*]acridines

Victoria Maroofi¹ · Mehdi Pordel¹ · Hamed Chegini¹ · Shirin Ramezani¹

Received: 24 April 2015 / Accepted: 30 June 2015 / Published online: 16 July 2015
© Springer Science+Business Media New York 2015

Abstract The new 3*H*-imidazo[4,5-*a*]acridine-11-carbonitriles were prepared from the reaction of 1-alkyl-5-nitro-1*H*-benzimidazoles with 2-(4-methoxyphenyl)acetonitrile and benzyl cyanide by nucleophilic substitution of hydrogen in high yields. Physical spectral and analytical data have confirmed the structures of the synthesized dyes. The optical and solvatochromic properties of these compounds were investigated and the results showed that they show very interesting photophysical properties. Density functional theory (DFT) calculations of fluorescent dyes were performed to provide the optimized geometries and relevant frontier orbitals. Furthermore, intra- and intermolecular interactions in fluorescent imidazo[4,5-*a*]acridines were evaluated by AIM (Atoms in Molecules) analysis.

Keywords 5-Nitro-1*H*-benzimidazole · Imidazo[4,5-*a*]acridine · Fluorescence · Emission and absorption spectra · Density functional theory · AIM analysis

Electronic supplementary material The online version of this article (doi:10.1007/s10895-015-1611-4) contains supplementary material, which is available to authorized users.

✉ Mehdi Pordel
mehdipordel58@yahoo.com

¹ Department of Chemistry, Mashhad Branch, Islamic Azad University, Mashhad, Iran

Introduction

Fluorescent heterocyclic compounds are of particular interest, because they exhibit unique electrical and optical properties such as emitters for electroluminescence devices [1], molecular probes for biochemical research [2], in traditional textile and polymer fields [3], fluorescent whitening agents [4] and photo conducting materials [5].

The concern with five-membered heterocyclic imidazole derivatives has been growing because these compounds have a number of optical applications, such as fluorescence compounds, dyes, and TPA materials (Two-photon absorption is the simultaneous absorption of two photons of identical or different frequencies in order to excite a molecule from one state to a higher energy electronic state) [6–8]. Furthermore, many commercial fluorescent brighteners for application to synthetic fibers contain an imidazole moiety [9].

On the other hand, acridine derivatives, as an important kind of tricycle nitrogen heterocycle, have been used for the production of dyes and some valuable drugs. Particularly, some of them are found to be efficient fluorescent chemosensors for recognition of transition metal ions such as Hg²⁺ [10] and emitters for luminescence studies [11]. Also, acridine orange (3,6-dimethylaminoacridine) is a nucleic acid-selective metachromatic stain valuable for cell cycle determination. Combination of the acridine moiety with the imidazole nucleus may enhance these properties.

Taking this body of research into consideration, we have synthesized some new imidazo[4,5-*a*]acridines with very interesting fluorescence properties. Density functional theory calculations (DFT) of fluorescent dyes were performed to provide the optimized geometries and relevant frontier orbitals. Intra- and intermolecular interactions in these fluorophores were also studied by AIM analysis.

Experimental

Materials

Methanol, *N,N*-Dimethylformamide (DMF), methyl iodide, benzyl chloride, ethyl bromide, *n*-propyl bromide, *n*-butyl bromide, iso-butyl bromide, 5-nitro-1*H*-benzimidazole, benzyl cyanide and 2-(4-methoxyphenyl)acetonitrile were purchased from Merck. Potassium hydroxide was purchased from Sigma-Aldrich. All solvents were dried according to standard procedures. Compounds **1a–f** were synthesized as in literature [12].

Equipment

Absorption and fluorescence spectra were recorded on a Varian 50-bio UV–visible spectrophotometer and a Varian Cary Eclipse spectrofluorophotometer. UV–vis and fluorescence scans were recorded from 350 to 700 nm. Melting points were measured on an Electrothermaltype-9100 melting-point apparatus. The IR (as KBr discs) spectra were obtained on a Tensor 27 spectrometer and only noteworthy absorptions are listed. The ^{13}C NMR (100 MHz) and the ^1H NMR (400 MHz) spectra were recorded on a Bruker Avance DRX-400 spectrometer in deuterated chloroform (CDCl_3). Chemical shifts are reported in parts per million downfield from tetramethylsilane (TMS) as the internal standard; coupling constant J is given in hertz. The mass spectra were recorded on a Varian Mat, CH-7 at 70 eV. Elemental analysis was performed on a Thermo Finnigan Flash EA microanalyzer. All measurements were carried out at room temperature.

Computational Methods

DFT calculations were performed with the Gaussian 98 software package [13] by using the B3LYP hybrid functional [14] and the 6-311++G(d,p) basis set. Firstly, geometry of the compound **3a** was fully optimized in the chloroform solution. The optimized geometry was confirmed to have no imaginary frequency. Then, its optimized geometry was used for frequency calculations.

Here, one of self-consistent reaction field methods, the sophisticated Polarized Continuum Model (PCM) [15] has been used for investigation of the solvent effects. The PCM calculations have been performed in the chloroform solution and the zero-point corrections were considered to obtain energies.

General Procedure for the Synthesis of **3a–g** from **1a–f** and **2a,b**

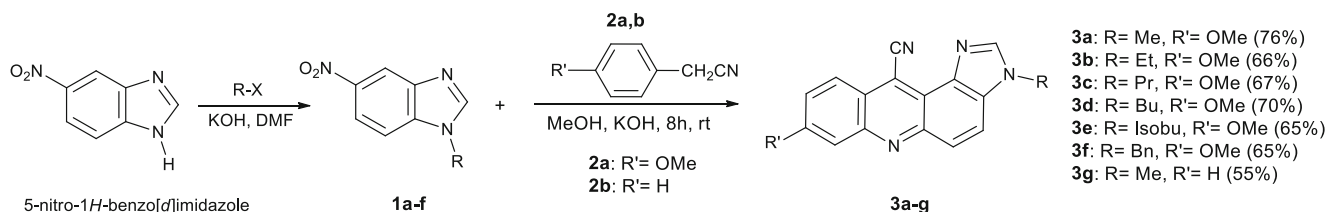
1-Alkyl-5-nitro-1*H*-benzimidazole **1a–f** (10 mmol) and **2a,b** (12 mmol) were added with stirring to a solution of KOH (20 g, 357 mmol) in methanol (50 mL). The mixture was

stirred at rt for 8 h. After concentration at reduced pressure, the precipitate was collected by filtration, washed with water, following with cold EtOH and acetone respectively, and then air dried to give crude **3a–g**. More purification was achieved by crystallization from suitable solvent such as MeOH or EtOH.

8-Methoxy-3-methyl-3*H*-imidazo[4,5-*a*]acridine-11-carbonitrile (3a**)** Compound **3a** was obtained as shiny yellow needles (EtOH), (76 %), m.p.: 320–322 °C; IR (KBr disk): CN 2240 cm^{-1} ; ^1H NMR: δ 4.03 (s, 3 H, OMe); 4.43 (s, 3 H, Me); 7.48 (dd, 1 H, H(9); $J_1=9.0$ Hz, $J_2=2.2$ Hz); 7.91 (d, 1 H, H(7), $J=2.2$ Hz); 8.06 (d, 1 H, H(10) $J=9.5$ Hz); 8.17 (s, 1 H, H(2)); 8.35 (d, 1 H, H(5) $J=9.0$ Hz); 8.43 (d, 1 H, H(4), $J=9.5$ Hz) ppm; ^{13}C NMR (125 MHz): δ 34.33, 56.37, 109.37, 111.23, 115.19, 116.9, 118.33, 120.31, 122.59, 124.63, 128.58, 130.97, 132.08, 139.59, 140.62, 146.11, 148.45 ppm; MS (EI, 70 eV), m/z (I_{rel} (%)): 288 $[\text{M}]^+$ (24); Found: C, 70.63; H, 4.16; N, 19.51. $\text{C}_{17}\text{H}_{12}\text{N}_4\text{O}$ (288.3) Calculated (%): C, 70.82; H, 4.20; N, 19.43.

3-Ethyl-8-methoxy-3*H*-imidazo[4,5-*a*]acridine-11-carbonitrile (3b**)** Compound **3b** was obtained as shiny yellow needles (EtOH), (66 %), m.p.: 288–289 °C; IR (KBr disk): CN 2240 cm^{-1} ; ^1H NMR: δ 1.62 (t, 3 H, CH_2CH_3 , $J=7.2$ Hz); 4.03 (s, 3 H, OMe); 4.41 (q, 2 H, CH_2CH_3 , $J=7.2$ Hz); 7.50 (dd, 1 H, H(9); $J_1=9.0$ Hz, $J_2=2.2$ Hz); 7.90 (d, 1 H, H(7), $J=2.2$ Hz); 8.08 (d, 1 H, H(10) $J=9.5$ Hz); 8.19 (s, 1 H, H(2)); 8.31 (d, 1 H, H(5) $J=9.0$ Hz); 8.43 (d, 1 H, H(4), $J=9.5$ Hz) ppm; ^{13}C NMR (125 MHz): δ 13.93, 36.90, 56.35, 109.38, 111.33, 115.20, 117.09, 118.42, 120.49, 122.51, 124.21, 128.69, 130.42, 131.87, 139.60, 140.63, 146.81, 148.42 ppm; MS (EI, 70 eV), m/z (I_{rel} (%)): 302 $[\text{M}]^+$ (27); Found: C, 71.39; H, 4.62; N, 18.65. $\text{C}_{18}\text{H}_{14}\text{N}_4\text{O}$ (302.3) Calculated (%): C, 71.51; H, 4.67; N, 18.53.

8-Methoxy-3-propyl-3*H*-imidazo[4,5-*a*]acridine-11-carbonitrile (3c**)** Compound **3c** was obtained as shiny yellow needles (MeOH), (67 %), m.p.: 268–270 °C; IR (KBr disk): CN 2240 cm^{-1} ; ^1H NMR: δ 1.01 (t, 3 H, $\text{CH}_2\text{CH}_2\text{CH}_3$, $J=7.0$ Hz); 1.89–2.01 (m, 2 H, $\text{CH}_2\text{CH}_2\text{CH}_3$); 4.03 (s, 3 H, OMe); 4.32 (t, 2 H, $\text{CH}_2\text{CH}_2\text{CH}_3$, $J=7.2$ Hz); 7.50 (dd, 1 H, H(9); $J_1=9.0$ Hz, $J_2=2.2$ Hz); 7.89 (d, 1 H, H(7), $J=2.2$ Hz); 8.08 (d, 1 H, H(10) $J=9.5$ Hz); 8.17 (s, 1 H, H(2)); 8.33 (d, 1 H, H(5) $J=9.0$ Hz); 8.42 (d, 1 H, H(4), $J=9.5$ Hz) ppm; ^{13}C NMR (125 MHz): δ 10.55, 24.78, 39.38, 56.34, 109.38, 111.27, 115.19, 116.94, 118.27, 120.48, 122.61, 124.62, 128.58, 130.97, 132.07, 139.59, 140.62, 146.95, 148.43 ppm; MS (EI, 70 eV), m/z (I_{rel} (%)): 316 $[\text{M}]^+$ (29). Found: C, 72.41; H, 5.15; N, 17.59. $\text{C}_{19}\text{H}_{16}\text{N}_4\text{O}$ (316.4) Calculated (%): C, 72.14; H, 5.10; N, 17.71.



Scheme 1 Synthesis of new fluorescent dyes **3a–g**

3-Butyl-8-methoxy-3H-imidazo[4,5-a]acridine-11-carbonitrile (3d) Compound **3d** was obtained as shiny yellow needles (MeOH), (70 %), m.p.: 260–262 °C; IR (KBr disk): CN 2240 cm^{-1} ; ^1H NMR: δ 0.98 (t, 3 H, $\text{CH}_2\text{CH}_2\text{CH}_2\text{CH}_3$, $J=7.0$ Hz); 1.29–1.39 (m, 2 H, $\text{CH}_2\text{CH}_2\text{CH}_2\text{CH}_3$); 1.89–2.01 (m, 2 H, $\text{CH}_2\text{CH}_2\text{CH}_2\text{CH}_3$); 4.02 (s, 3 H, OMe); 4.27 (t, 2 H, $\text{CH}_2\text{CH}_2\text{CH}_2\text{CH}_3$, $J=7.1$ Hz); 7.49 (dd, 1 H, H(9); $J_1=9.0$ Hz, $J_2=2.2$ Hz); 7.89 (d, 1 H, H(7), $J=2.2$ Hz); 8.09 (d, 1 H, H(10) $J=9.5$ Hz); 8.16 (s, 1 H, H(2)); 8.32 (d, 1 H, H(5) $J=9.0$ Hz); 8.43 (d, 1 H, H(4), $J=9.5$ Hz) ppm; ^{13}C NMR (125 MHz): δ 13.94, 18.65, 33.45, 38.48, 56.34, 109.55, 111.1, 115.20, 116.76, 118.01, 120.55, 122.50, 124.60, 128.90, 130.44, 132.19, 139.71, 140.62, 146.97, 148.41 ppm; MS (EI, 70 eV), m/z (I_{rel} (%)): 330 $[\text{M}]^+$ (33); Found: C, 72.59; H, 5.43; N, 17.09. $\text{C}_{20}\text{H}_{18}\text{N}_4\text{O}$ (330.4) Calculated (%): C, 72.71; H, 5.49; N, 16.96.

3-Isobutyl-8-methoxy-3H-imidazo[4,5-a]acridine-11-carbonitrile (3e) Compound **3e** was obtained as shiny yellow needles (MeOH), (70 %), m.p.: 260–262 °C; IR (KBr disk): CN 2240 cm^{-1} ; ^1H NMR: δ 0.90 (d, 6 H, $\text{CH}_2\text{CH}(\text{CH}_3)_2$, $J=6.4$ Hz); 2.15–2.19 (m, 1H, $\text{CH}_2\text{CH}(\text{CH}_3)_2$); 4.32 (d, 2H, $\text{CH}_2\text{CH}(\text{CH}_3)_2$, $J=7.2$ Hz); 7.48 (dd, 1 H, H(9); $J_1=9.0$ Hz,

$J_2=2.2$ Hz); 7.90 (d, 1 H, H(7), $J=2.2$ Hz); 8.08 (d, 1 H, H(10) $J=9.5$ Hz); 8.14 (s, 1 H, H(2)); 8.33 (d, 1 H, H(5) $J=9.0$ Hz); 8.44 (d, 1 H, H(4), $J=9.5$ Hz) ppm; ^{13}C NMR (125 MHz): δ 20.42, 29.80, 58.91, 109.51, 110.80, 115.28, 116.79, 117.97, 120.53, 122.51, 124.62, 128.91, 130.42, 132.18, 139.73, 140.65, 146.95, 148.44 ppm; MS (EI, 70 eV), m/z (I_{rel} (%)): 330 $[\text{M}]^+$ (39); Found: C, 72.89; H, 5.53; N, 16.86. $\text{C}_{20}\text{H}_{18}\text{N}_4\text{O}$ (330.4) Calculated (%): C, 72.71; H, 5.49; N, 16.96.

3-Benzyl-8-methoxy-3H-imidazo[4,5-a]acridin-11-carbonitrile (3f) Compound **3f** was obtained as shiny yellow needles, (65 %), m.p.: 273–275 °C; IR (KBr disk): CN 2240 cm^{-1} ; ^1H NMR: δ 4.03 (s, 3 H, OMe); 5.41 (s, 2 H, CH_2Ph); 7.13–7.25 (m, 5 H, Ar); 7.48 (dd, 1 H, H(9); $J_1=9.0$ Hz, $J_2=2.2$ Hz); 7.91 (d, 1 H, H(7), $J=2.2$ Hz); 8.06 (d, 1 H, H(10) $J=9.5$ Hz); 8.18 (s, 1 H, H(2)); 8.34 (d, 1 H, H(5) $J=9.0$ Hz); 8.44 (d, 1 H, H(4), $J=9.5$ Hz) ppm; ^{13}C NMR (125 MHz): δ 49.35, 56.37, 109.31, 111.40, 115.18, 116.87, 118.23, 118.69, 120.53, 122.62, 122.79, 123.76, 124.61, 125.03, 128.59, 130.99, 132.07, 139.58, 140.62, 146.53, 148.43 ppm. MS (EI, 70 eV), m/z (I_{rel} (%)): 364 $[\text{M}]^+$ (21);

Scheme 2 The reaction mechanism for the formation of **3a–g**

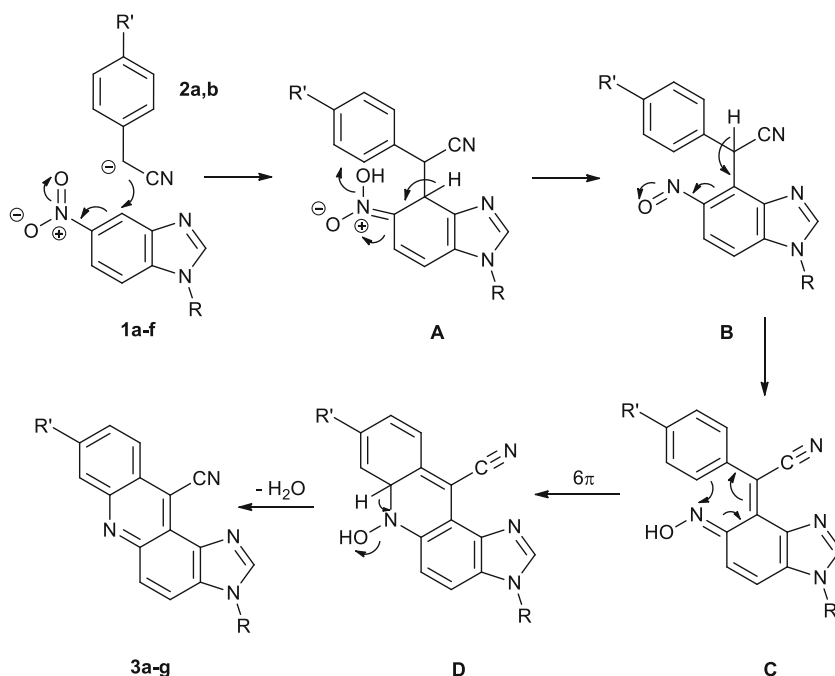


Table 1 Spectroscopic data for green fluorescent **3a–g** at 298 K

Dye	3a	3b	3c	3d	3e	3f	3g
λ_{abs} (nm) ^a	385	385	385	385	385	390	375
$\epsilon \times 10^{-4}$ [(mol L ⁻¹) ⁻¹ cm ⁻¹] ^b	29.2	31.5	37.1	29.4	39.2	37.8	17.3
λ_{ex} (nm) ^c	380	380	380	380	380	380	380
λ_{flu} (nm) ^d	480	485	480	480	480	485	455
Φ_{F} ^e	0.92	0.93	0.93	0.92	0.87	0.94	0.61

^a Wavelengths of maximum absorbance (λ_{abs})^b Extinction coefficient^c Wavelengths of fluorescence excitation (λ_{ex})^d Wavelengths of fluorescence emission (λ_{flu})^e Fluorescence quantum yield

Found: C, 75.65; H, 4.38; N, 15.51. C₂₃H₁₆N₄O (364.4) Calculated (%): C, 75.81; H, 4.43; N, 15.37.

3-Methyl-3*H*-imidazo[4,5-*a*]acridin-11-carbonitrile (**3 g**)

Compound **3 g** was obtained as shiny yellow needles, (55 %), m.p.: 245–247 °C; IR (KBr disk): CN 2240 cm⁻¹; ¹H NMR: δ 4.35 (s, 3 H, Me); 7.69–7.80 (m, 3 H, Ar), 8.11 (d, 1 H, $J=9.0$ Hz, Ar-H), 8.20 (s, 1 H, Ar-H), 8.49 (d, 1 H, $J=9.0$ Hz, Ar-H), 8.57 (dd, 1 H, $J=8.4, 1.2$ Hz, Ar-H), ppm; ¹³C NMR (CDCl₃): δ 37.34, 112.72, 115.83, 117.49, 121.45, 123.19, 127.29, 128.64, 132.28, 132.89, 135.21, 136.10, 136.65, 137.50, 141.81, 147.33 ppm. MS (m/z) 258 (M⁺). Anal. Calcd for C₁₆H₁₀N₄ (258.3): C, 74.41; H, 3.90; N, 21.69. Found: C, 74.71; H, 3.95; N, 21.39.

Results and Discussion

Synthesis and Structures of the New Compounds **3a–g**

The precursors of 1-alkyl-5-nitro-1*H*-benzimidazoles (**1a–f**) were obtained from the reaction of 5-nitro-1*H*-benzimidazole

with different alkyl halides at room temperature in DMF in the presence of KOH [12]. The new 3*H*-imidazo[4,5-*a*]acridin-11-carbonitriles **3a–g** were synthesized via the nucleophilic substitution of hydrogen of *N*-alkylated 5-nitrobenzimidazoles **1a–f** with arylacetonitriles **2a,b** in basic MeOH solution and following with subsequent cyclization and dehydration and in excellent yields at room temperature (Scheme 1). One of the noteworthy points in this reaction was the simple work-up procedure performed by filtration of the precipitated product after the mixture was concentrated at reduced pressure. Washing the precipitated product with suitable solvents (water, EtOH and then acetone) gives practically pure compounds **3a–g**.

A tentative mechanism to explain the formation of compounds **3a–g** is shown in Scheme 2. The ring closure proceeding occurs via an electrocyclic pathway, wherein intermediate **C** converted to **D** and following with dehydration, compounds **3a–g** are obtained [16–18].

The structural assignments of compounds **3a–g** were based on the analytical and spectral data. For example, in the ¹H NMR spectrum of **3a** revealed the doublet of doublet signal at δ_{H} 7.48 ppm ($J_1=9.0$ Hz and $J_2=2.2$ Hz), the doublet signals at δ 7.91 ppm with meta J (2.2 Hz), δ_{H} 8.06 ppm, δ_{H} 8.35 ppm and δ_{H} 8.43 ppm and singlet signal at δ_{H} 8.17 ppm assignable to six protons of aromatic rings. Moreover, the FT-IR spectrum of **3a** in KBr showed an absorption band at 2240 cm⁻¹ corresponding to cyanide group. Furthermore, the mass spectrum of this product shows the molecular ion m/z 288 (M⁺), confirming its presumed structure. Analytical data are also in accordance with the proposed tetracyclic structure for compound **3a**.

Photophysical Properties of **3a–g**

The compounds **1a–f**, **2a,b** and **3a–g** were spectrally characterized by using an UV–vis spectrophotometer and a

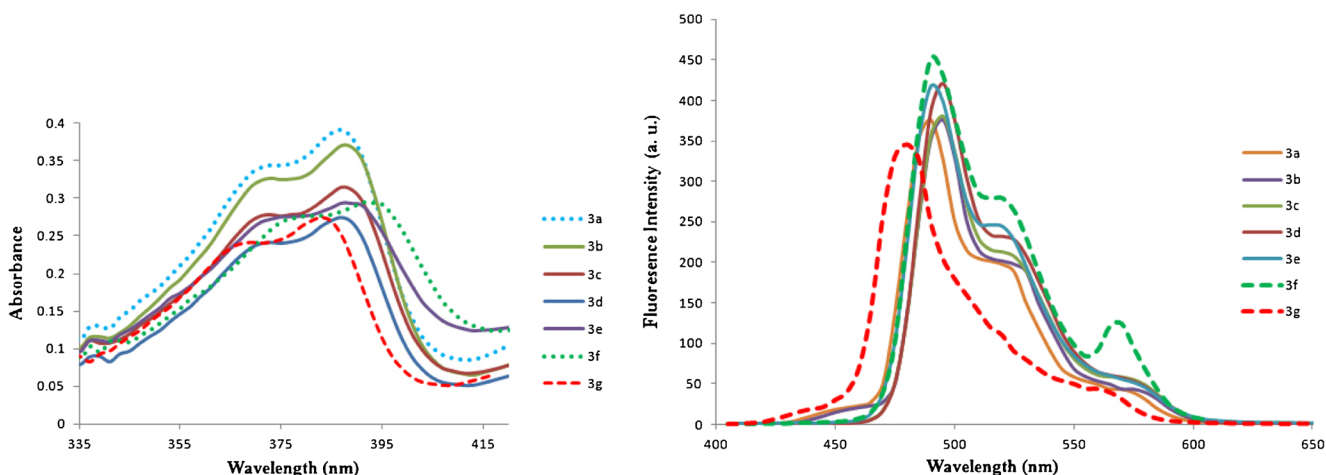


Fig. 1 Visible absorption (*left*) and emission spectra (*right*) of compounds **3a–g** in chloroform solvent

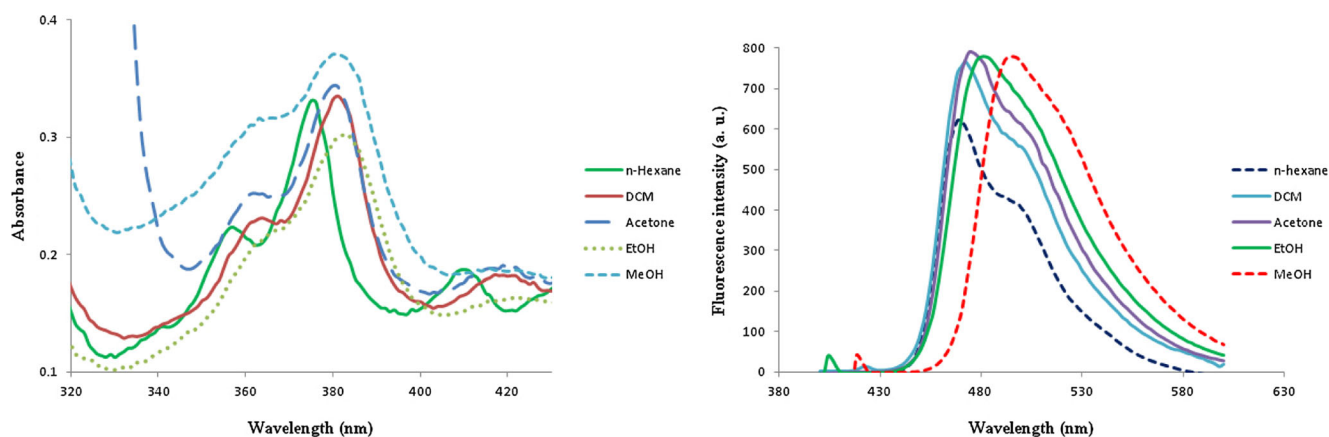


Fig. 2 Visible absorption (2×10^{-6} mol L $^{-1}$) and emission spectra (3×10^{-7} mol L $^{-1}$) of compound **3a** in different solvents

fluorescence spectrophotometer. The wavelength range of both spectrophotometers is 200 nm–1000 nm. The emission spectra of the precursors **1a–f** and **2a,b** don't show any fluorescence emission peaks even at high concentrations. The fluorescence absorption and emission spectra of **3a–g** were recorded at concentrations of 2×10^{-6} and 1×10^{-7} mol L $^{-1}$ in chloroform, respectively. Numerical data are presented in Table 1; Fig. 1 shows the visible absorption and emission spectra of compounds **3a–g**.

Values of extinction coefficient (ϵ) were calculated as the slope of the plot of absorbance vs concentration. The fluorescence excitation (λ_{ex}) wavelength at 380 nm ($\lambda_{\text{ex}}/\text{nm}$) was used for all compounds **3a–g**. The fluorescence quantum yields (Φ_{F}) of compounds **3a–g** were determined via comparison methods, using fluorescein as a standard sample in 0.1 M NaOH and MeOH solution [19]. The used value of the fluorescein emission quantum yield is 0.79. The absorbance and fluorescence spectral properties (Table 1) of compounds **3a–g** are similar to each other and the Φ_{F} of **3f** (R=Bn) was the highest.

The intramolecular charge transfer (ICT) states from the donor endocyclic nitrogen to the acceptor CN group can be considered as the main reason for the fluorescence intensity of green fluorescent **3a–g** [17, 18].

The solvatochromic properties of compound **3a** were deduced from Fig. 2. The fluorescence absorption and emission spectra of **3a** in polar solvents undergo a relatively modest red shift. Increasing the solvent polarity stabilizes the ICT excited-state molecule relative to the ground-state molecule with the observed red shift of the absorption maximum as the experimentally observed result (Table 2). For example, in the absorption and emission spectra of compound **3a**, λ_{abs} and λ_{flu} shift from 375 to 395 nm and 465 to 500 nm respectively, as the solvent changes from *n*-hexane to methanol (Table 2).

DFT Calculations

The Φ_{F} of **3a–f** are the highest quantum yield values among the fluorescent imidazo[4,5-*a*]acridines which we have

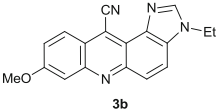
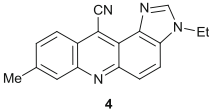
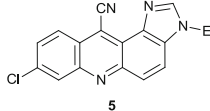
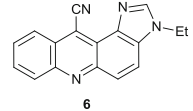
previously synthesized [17, 18]. Furthermore, values of extinction coefficient (ϵ) of **3a–f** are greater than latter compounds. A comparison of photophysical data between **3b** and some of these is shown in Table 3. To gain a deeper insight into the role of 8-substituent in the charge transfer properties of imidazo[4,5-*a*]acridine derivatives, we performed DFT calculations at the B3LYP/6-311++G(d,p) level and obtained the optimized geometries and HOMO (highest occupied molecular orbital) and LUMO (lowest unoccupied molecular orbital) (frontier orbitals of fluorescent imidazo[4,5-*a*]acridines). The optimized geometries of compounds **3b**, **4**, **5**, and **6** can be found in Supplementary data (Figure S1).

The energy difference between the HOMO and LUMO frontier orbitals is one of the important characteristics of molecules, which has a determining role in such cases as electric properties, electronic spectra and photochemical reactions. The HOMO and LUMO maps of **3b**, **4**, **5**, and **6** are shown in Fig. 3. Separation energies between the HOMO and LUMO ($\Delta\epsilon = \epsilon_{\text{LUMO}} - \epsilon_{\text{HOMO}}$) in dyes **3b**, **4**, **5**, and **6** are 3.08, 3.25, 3.19 and 3.24 eV, respectively. Role of the 8-substituent on the $\Delta\epsilon$ of imidazo[4,5-*a*]acridines can be analyzed by comparing the estimated energy HOMO and LUMO levels in compounds **3b**, **4**, **5**, and **6**. The results show that the separation energy between the HOMO and LUMO in compound **3b** is lower compared with compounds **4**, **5**, and **6**. This implies that the energy levels of the HOMO in compound **3b** are higher than those of compounds **4**, **5**, and **6**, because of the higher electron density caused by 8-methoxy substituent. In spite of electronegativity of chlorine, the separation energy between the

Table 2 Spectroscopic data for compound **3a** at 298 K in different solvent

Solvent	λ_{abs} (nm)	λ_{flu} (nm)
<i>n</i> -hexane	375	465
DCM	385	470
Acetone	390	485
EtOH	390	490
MeOH	395	500

Table 3 Comparison of the photophysical properties of **3b** and some recently synthesized fluorescent imidazo[4,5-*a*]acridines

Compound				
λ_{abs} (nm)	385	380	380	375
$\epsilon \times 10^{-4}$ [(mol L ⁻¹) ⁻¹ cm ⁻¹]	29.2	14.7	27.5	17.3
λ_{flu} (nm)	480	460	488	455
Φ_{F}	0.92	0.75	0.86	0.61

HOMO and LUMO in compound **4** is lower than $\Delta\epsilon$ in dyes **5** and **6**, confirming chlorine atom donates a pair of electrons to the aromatic ring which increases the energy levels of the HOMO. Comparing the photophysical properties in Table 4 reveals that the values of quantum yield and extinction coefficient are in good agreement with the separation energy between the HOMO and LUMO of dyes **3b**, **4**, **5**, and **6**.

AIM Analysis

The Bader theory comes of ages as a very useful tool to analyze intra- and intermolecular interactions.

The cyano fragment, having a completely planar structure, plays an acceptor role of the photo excited electron in the dye molecules and their derivatives.

The presence of the intramolecular interactions $N_{(9)} \cdots C_{(CN)}$ and different concentration of electron density through the C-N bond in the cyano fragment in the four derivatives of imidazo[4,5-*a*]acridine-11-carbonitrile dyes were proved in the current study via reasoning from the existence of the four different substituents.

To evaluate the intramolecular interaction energy the following equation, which is given by Espinosa et al. [20], has

been used. According to the properties of electron density distribution in the BCP (bond critical point) we have [21]:

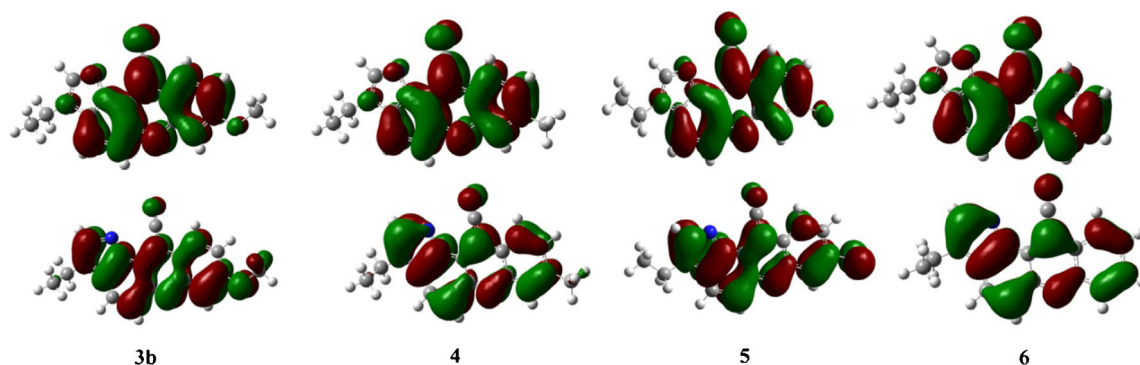
$$E, au = 0.5 V,$$

Where V is the local potential energy value for interaction at BCP.

The parameters such as the Laplacian of the electron density $\nabla^2\rho$, the electron energy density H_C , the sum of the kinetics electron energy density (G_C) and the potential electron energy density (V_C), and as well as $-G_C/V_C$, derive from the Bader theory and imply the interaction type and changing stability of bond after molecular rotate, intermolecular or intra-molecular interactions.

For a negative value of a Laplacian, $\nabla^2\rho < 0$ beyond doubt the interaction is completely covalent. If both $\nabla^2\rho$ and H_C be simultaneously positive ($\nabla^2\rho(r) > 0, H_C > 0$) which can be categorized as the interactions of closed electron shells, to which, in particular, most hydrogen bonds and van der Waals interactions belong. If $\nabla^2\rho$ be positive while H_C is negative, and the $-G_C/V_C$ is smaller than 1, then the nature of interaction is considered as partly covalent [22].

The topological parameters, such as ρ_{BCP} , $\nabla^2\rho$, G_C , V_C , ($-G_C/V_C$) and H_C at the BCP of $N \cdots C$, $C - N$ and $C - R$ (R' :

**Fig. 3** The HOMO (down) and LUMO (up) frontier orbitals of the compounds **3a**, **4**, **5** and **6**

OCH₃, CH₃, Cl, H) for compounds **3b**, **4**, **5**, and **6** are represented in Table 4. The molecular graphs with electron density iso-surface map of all 4 derivatives are given in Fig. 4. It appears from the molecular graphs that there are a BCP between the C ⋯ N atoms, which are connected through two bond paths. The topological structure shows that the intramolecular C ⋯ N bond existed in the structure of molecule imidazo[4,5-*a*]acridine. From the data shown in Table 4, the following results can be drawn: for the BCP of the C ⋯ N, the $\nabla^2\rho$, H_C are positive, and the ratio of G_C to V_C , $-G_C/V_C$, ranges up than 1; therefore, all values of topological

parameters imply that the intramolecular C ⋯ N bond, is rather van der Waals in all derivatives of imidazo[4,5-*a*]acridine [23–25], and all intramolecular interactions are same too. From Table 4, it seems that due to a decrease electron donating of substituent groups which is located at the bond path, ρ_{BCP} at the BCP increased. It is deserve to mention that intramolecular interactions bond stronger than other interactions in the structures.

In other hands, it seems that due to an increase in the electron withdrawing order of substituent groups, E at the BCP increased, which shows that the bond path's order of

Table 4 Topological properties at the BCP for compounds **3b**, **4**, **5**, and **6**

	BCP #	$ q(A,B) $	$\delta(A,B)$	BPL	Atoms	ρ	$\nabla^2\rho$	G	V	$-G/V$	H
Cl	8	0.28005	1.068583	2.604173	C4 - N7	0.302908	-0.73835	0.231963	-0.64851	0.357684	-0.41655
	9	0.087655	1.233313	2.644262	C4 - C5	0.313131	-0.87054	0.103596	-0.42483	0.243855	-0.32123
	11	0.506356	0.887542	2.781873	N7 - C10	0.245745	-0.59397	0.138639	-0.42577	0.325619	-0.28713
	12	0.084859	0.98655	2.878681	C10 - C11	0.244155	-0.56271	0.056493	-0.25366	0.222709	-0.19717
	14	0.414337	1.19074	2.599986	C5 - N9	0.318359	-0.91991	0.175693	-0.58136	0.302209	-0.40567
	17	0.002815	0.037104	5.639897	N9 - C21	0.009409	0.033447	0.00691	-0.00546	1.2658	0.001451
	29	0.210371	1.099566	3.322686	C18 - Cl20	0.191923	-0.26859	0.063902	-0.19495	0.327783	-0.13105
	30	0.260445	1.084264	2.703007	C12 - C21	0.27924	-0.76006	0.083659	-0.35733	0.23412	-0.27368
	31	1.13883	2.334288	2.184176	C21 - N22	0.477335	-0.30141	0.784144	-1.64364	0.477078	-0.8595
	H	8	0.084431	1.234943	2.645742	C4 - C5	0.31265	-0.86726	0.103469	-0.42375	0.244173
9		0.285169	1.066862	2.604556	C4 - N7	0.302237	-0.735	0.23148	-0.64671	0.357935	-0.41523
11		0.373004	1.070635	2.589971	N7 - C8	0.308883	-0.76158	0.240896	-0.67219	0.358377	-0.43129
12		0.417581	1.188011	2.603205	C5 - N9	0.316985	-0.91277	0.174874	-0.57794	0.302581	-0.40307
14		0.671488	1.379856	2.484972	C8 - N9	0.362699	-1.07305	0.261923	-0.79211	0.330665	-0.53019
19		0.002357	0.037039	5.640526	N9 - C20	0.009416	0.033453	0.00691	-0.00546	1.266264	0.001453
29		0.041258	0.957627	2.020016	C18 - H32	0.282962	-0.97966	0.036827	-0.31857	0.115601	-0.28174
32		0.268173	1.085454	2.702372	C12 - C20	0.279229	-0.75966	0.084305	-0.35852	0.235145	-0.27422
33		1.145048	2.330719	2.184441	C20 - N21	0.477249	-0.30641	0.782574	-1.64175	0.47667	-0.85918
OCH ₃		7	0.286852	1.064436	2.6063	C4 - N7	0.301526	-0.73127	0.230945	-0.64471	0.358216
	8	0.081118	1.237136	2.644437	C4 - C5	0.313012	-0.86892	0.103782	-0.42479	0.244311	-0.32101
	12	0.373557	1.072858	2.588329	N7 - C8	0.309287	-0.75991	0.242538	-0.67505	0.359287	-0.43252
	13	0.42169	1.188795	2.602723	C5 - N9	0.317066	-0.91292	0.175398	-0.57903	0.302919	-0.40363
	14	0.668583	1.377515	2.486224	C8 - N9	0.362247	-1.07323	0.260282	-0.78887	0.329942	-0.52859
	16	0.001868	0.036996	5.643166	N9 - C22	0.009393	0.033324	0.006886	-0.00544	1.265809	0.001446
	28	0.499396	0.932664	2.571955	C18 - O20	0.28704	-0.3735	0.314767	-0.72291	0.435417	-0.40814
	31	0.270641	1.084047	2.703429	C12 - C22	0.278919	-0.75875	0.084137	-0.35796	0.235044	-0.27383
	32	1.146511	2.330937	2.184609	C22 - N23	0.477169	-0.30775	0.782002	-1.64094	0.476557	-0.85894
	CH ₃	8	0.082033	1.234838	2.645758	C4 - C5	0.312644	-0.86726	0.103445	-0.4237	0.244145
9		0.286169	1.065296	2.605487	C4 - N7	0.301895	-0.73381	0.231021	-0.64549	0.357899	-0.41447
12		0.373446	1.071344	2.589392	N7 - C8	0.309007	-0.76111	0.241371	-0.67302	0.358638	-0.43165
13		0.419815	1.187717	2.603362	C5 - N9	0.316897	-0.91242	0.174873	-0.57785	0.302626	-0.40298
14		0.670123	1.379326	2.48518	C8 - N9	0.362648	-1.07371	0.261418	-0.79126	0.330381	-0.52984
17		0.002035	0.036917	5.643576	N9 - C21	0.009393	0.033358	0.00689	-0.00544	1.266311	0.001449
29		0.072906	1.018234	2.846452	C18 - C20	0.251519	-0.59958	0.058816	-0.26753	0.219851	-0.20871
31		0.270909	1.084954	2.703026	C12 - C21	0.278994	-0.75871	0.084293	-0.35826	0.235282	-0.27397
32		1.146833	2.330638	2.184631	C21 - N22	0.477154	-0.30806	0.781884	-1.64078	0.476531	-0.8589

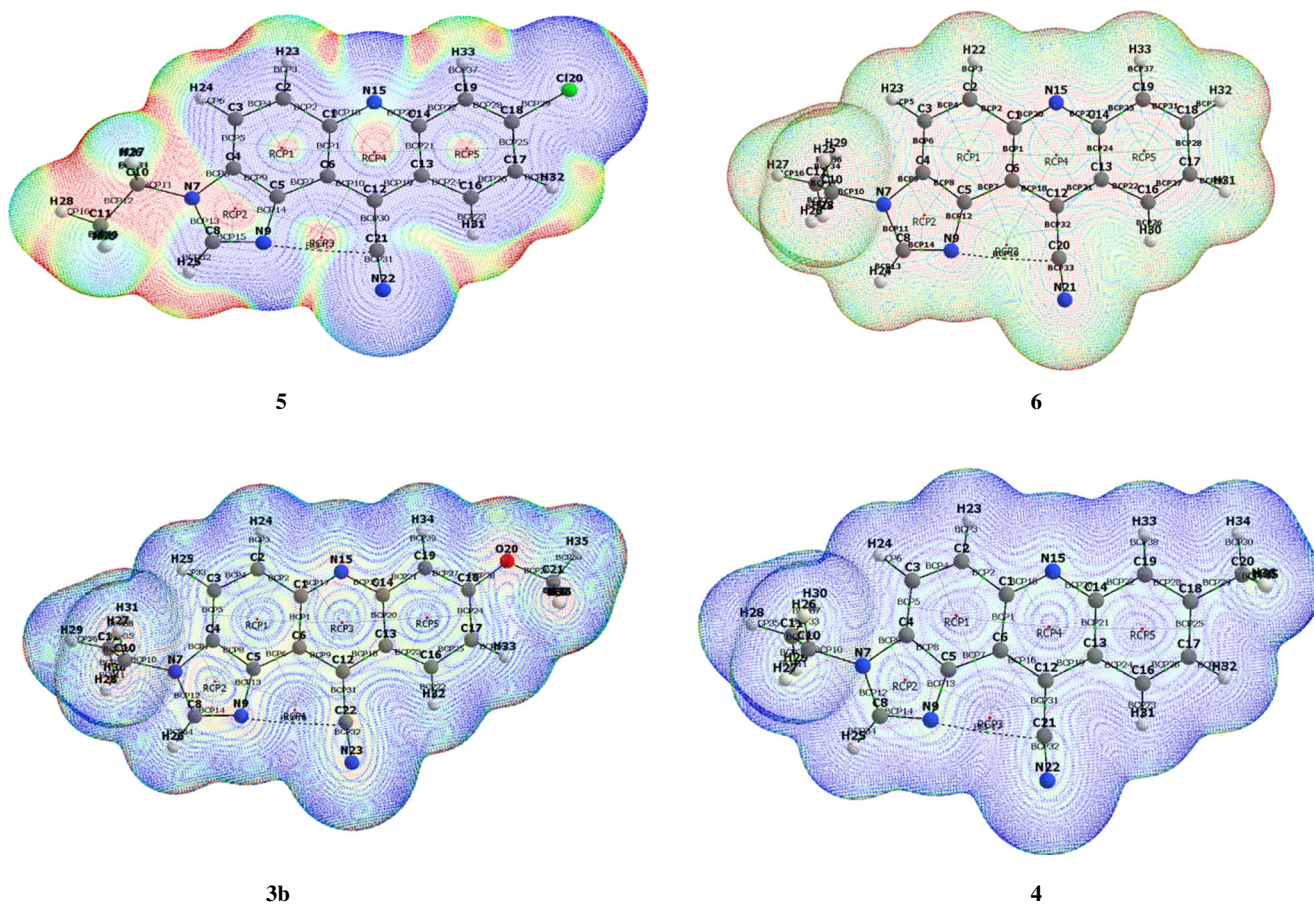


Fig. 4 Electron density iso-surface map of compounds **3b**, **4**, **5**, and **6**

magnitude is, respectively, OCH₃, CH₃, H and Cl is strongest.

According to Table 4, the intramolecular interaction of cyano-imidazole affected by order of the electron donating of substituent, which decrease of the electron withdrawing and increases of electron donating of substituents, intramolecular interaction could be stronger, but it is not very obvious, because the substituent is far from the located interaction, so has negligible effect of substituents affected by resonance of ring, that is could be a weak.

The RCP (ring critical point) is a point of minimum electron density within the ring surface and a maximum on the ring line [26, 27]. Table 5 gives the information about electron density ρ_{RCP} at the RCP and $\nabla^2 \rho_{RCP}$ of the chelate ring, produced by the intra-intermolecular interaction formation.

From Table 5, the value of the electron density ρ_{RCP} , $\nabla^2 \rho_{RCP}$ and K reason this fact that imidazole ring is stable with the electron withdrawing substituent.

So, electron donating effect of imidazole ring could be more charged by the electron withdrawing substituent.

Table 5 The topological properties at the RCP for **3b**, **4**, **5**, and **6**

	RCP #	Atoms	ρ	$\nabla^2 \rho$	K
Cl	2	-C4 - C5 - N9 - C8 - N7-	0.056	0.391492	-0.00568
	3	-C5 - C6 - C12 - C21 - N9-	0.008929	0.04224	-0.00227
H	2	-C4 - C5 - N9 - C8 - N7-	0.055941	0.391679	-0.00573
	3	-C5 - C6 - C12 - C20 - N9-	0.008924	0.042292	-0.00228
OCH ₃	2	-C4 - C5 - N9 - C8 - N7-	0.055937	0.391678	-0.00573
	4	-C5 - C6 - C12 - C22 - N9-	0.008905	0.042155	-0.00227
CH ₃	2	-C4 - C5 - N9 - C8 - N7-	0.055923	0.391541	-0.00573
	3	-C5 - C6 - C12 - C21 - N9-	0.008904	0.04216	-0.00227

Conclusion

In conclusion, we have synthesized seven new green fluorescent heterocyclic imidazo[4,5-*a*]acridines in excellent yields which demonstrate interesting optical properties including high extinction coefficients and a very high quantum yield. DFT calculations were performed to gain a deeper insight into the charge transfer properties by using the B3LYP hybrid functional and the 6-311++G(d,p) basis set. The results showed that the geometry of imidazo[4,5-*a*]acridine dyes was rigid and planar and the separation energies between the HOMO and LUMO in dyes **3b**, **4**, **5** and **6** were 3.08, 3.25, 3.19 and 3.24 eV, respectively. In addition, AIM analysis was conducted to investigate intra- and intermolecular interactions in these fluorophores. The results show that there are the intramolecular interactions $N_{(9)} \cdots C_{(CN)}$ and different concentration of electron density through the C-N bond in the cyano fragment in the four derivatives of imidazo[4,5-*a*]acridines. The effect of electron donating and electron withdrawing of substituents on the intramolecular interactions in compounds **3b**, **4**, **5** and **6** were also studied.

Because of the use of fluorescence for imaging in the biological and material science fields, further synthetic and fluorescence studies are necessary on similar substrates to expand this field of knowledge and establish sound conclusions. For example, the ability of attaching of fluorophores **3a-f** into biologically active compounds can be increased with converting their methoxy substituent to hydroxyl group. This work is in progress.

References

- Hunger K (2003) In *industrial dyes*. WILEY-VCH Verlag, Weinheim, pp 569–572
- Dmitry A, Pavel A (2003) Dipyrrolyl quinoxalines with extended chromophores are efficient fluorimetric sensors for pyrophosphate. *Chem Commun* 12:1394
- Gold H, Venkataraman H (1971) Ed. Pergamon, New York, Academic Press, pp 535–542
- Belgodere E, Bossio R, Chimichi S, Passini V, Pepino R (1985) Synthesis and fluorescence of some thiazole and benzothiazole derivatives. *Dyes Pigments* 4:59
- Kalle AG (1962) British patent, 895(001). *Chem Abstr* 57:14578
- Fridman N, Kaftory M, Speiser S (2007) Structures and photophysics of lophine and double lophine derivatives. *Sensors Actuators B* 126:107
- Karolak-Wojciechowska J, Mrozek A, Czykowski R, Tekiner-Gulbas B, Ak-Sener E, Yalcin I (2007) Crystal structure and molecular mechanics modelling of 2-(4-Amino-3-benzyl-2-thioxo-2,3-dihydrothiazol-5-yl)benzoxazole. *J Mol Struct* 839:125
- Pan WL, Tan HB, Chen Y, Mu DH, Liu HB, Wan YQ et al (2008) The synthesis and preliminary optical study of 1-alkyl-2,4,5-triphenylimidazole derivatives. *Dyes Pigments* 76:17
- Um SI (2007) The synthesis and properties of benzoxazole fluorescent brighteners for application to polyester fibers. *Dyes Pigments* 75:185
- Karagöz F, Güney O, Kandaz M, Bilgiçli AT (2012) Acridine-derived receptor for selective mercury binding based on chelation-enhanced fluorescence effect. *J Lumin* 132:2736
- Ferreira APG, Frederice R, Janssen KPF, Gehlen MH (2011) Dually fluorescent silica nanoparticles. *J Lumin* 131:888
- Preston P N (1980) The chemistry of heterocyclic compounds, benzimidazoles and cogeneric tricyclic compounds. John Wiley & Sons, Part 1, Volume 40, pp 87–105
- Frisch MJ, Trucks GW, Schlegel HB, Scuseria GE et al (1998) Gaussian 98, revision A.7. Gaussian, Inc, Pittsburgh PA
- Lee C, Yang W, Parr RG (1988) Development of the Colle-Salvetti correlation-energy formula into a functional of the electron density. *Phys Rev B* 37:785
- Tomasi J, Cammi R (1995) Remarks on the use of the apparent surface charges (ASC) methods in solvation problems: iterative versus matrix-inversion procedures and the renormalization of the apparent charges. *J Comput Chem* 16:1449
- Davis RB, Pizzini LC (1960) Condensation of aromatic nitro compounds with acrylacetonitriles. *J Org Chem* 25:1884
- Sahraei R, Pordel M, Behmadi H, Razavi B (2013) Synthesis of a new class of strongly fluorescent heterocyclic compounds: 3H-imidazo [4, 5-*a*] acridine-11-carbonitriles. *J Lumin* 136:334
- Pordel M (2012) Synthesis of new fluorescent compounds from benzimidazole. *J Chem Res* 36:595
- Umberger JQ, LaMer VK (1945) The kinetics of diffusion controlled molecular and ionic reactions in solution as determined by measurements of the quenching of fluorescence. *J Am Chem Soc* 67:1099
- Espinosa E, Molins E (2000) About the evaluation of the local kinetic, potential and total energy densities in closed-shell interactions. *J Chem Phys* 113:5686
- Bader R F (1990) Atoms in molecules: a quantum theory. International series of monographs on chemistry 22, in, Oxford University Press, Oxford
- Vener M, Manaev A, Egorova A, Tsirelson V (2007) QTAIM study of strong H-bonds with the $OH\odot\odot\odot A$ Fragment ($A=O, N$) in three-dimensional periodical crystals. *J Phys Chem A* 111:1155
- Mata I, Alkorta I, Molins E, Espinosa E (2010) Universal features of the electron density distribution in hydrogen-bonding regions: a comprehensive study involving $H\cdots X$ ($X=H, C, N, O, F, S, Cl, \pi$) interactions. *Chem Eur J* 16:2442
- Krygowski TM, Zachara-Horeglad JE, Palusiak M, Pelloni S, Lazzaretto P (2008) Relation between π -electron localization/delocalization and H-bond strength in derivatives of o-hydroxy-Schiff Bases. *J Org Chem* 73:2138
- Li X, Wang Y, Zheng S, Meng L (2012) Substituent effects on the intramolecular hydrogen bond in 1-hydroxyanthraquinone: AIM and NBO analyses. *Struct Chem* 23:1233
- Bader RF, Carroll MT, Cheeseman JR, Chang C (1987) Properties of atoms in molecules: atomic volumes. *J Am Chem Soc* 109:7968
- Mitra S, Chandra AK, Gashnga PM, Jenkins S, Kirk SR (2012) Exploring hydrogen bond in the excited state leading toward intramolecular proton transfer: detailed analysis of the structure and charge density topology along the reaction path using QTAIM. *J Mol Model* 18:4225